0038-075C/00/16503-237–249
Soil Science

March 2000
Vol. 165, No. 3
Printed in U.S.A.

NLOSS: A MECHANISTIC MODEL OF DENITRIFIED N_2O AND N_2 EVOLUTION FROM SOIL

W. J. Riley[1] and P. A. Matson[2]

Soil microbial denitrification is a significant source of atmospheric nitrous oxide (N_2O), a trace gas important in global climate change and stratospheric ozone depletion. In this paper we describe a mechanistic submodel, which is incorporated in the model NLOSS, designed to predict the soil biogenic source and efflux of N_2O and N_2 during denitrification. NLOSS simulates transient soil moisture and temperature, decomposition, soil anaerobicity, denitrifying bacterial biomass, rates of soil nitrogen transformations, soil trace-gas transport, and gas efflux to the atmosphere. Uncertainty in predicted N gas effluxes is computed using a Monte Carlo approach. We test NLOSS's denitrification estimates by comparing predictions with results from a ^{15}N tracer experiment in a Mexican agricultural system. The model accurately predicted the measured soil moisture and denitrified N_2O and N_2 fluxes during the experiment. We also apply NLOSS to compute denitrified N trace-gas speciation curves as a function of soil hydrologic properties and moisture content. These speciation curves will be used in future work to extrapolate the plot-scale modeling results presented here to field and regional estimates of N trace-gas emissions. The results presented here suggest that NLOSS can be used to identify the processes most important for trace-gas losses and to facilitate efforts to scale plot-level modeling results to regional estimates of N trace-gas emissions. (Soil Science 2000;165:237–249)

Key words: denitrification, N_2O flux, N_2 flux, nitrogen cycling, modeling.

THE intensification of agriculture has led to significant environmental consequences. Globally, N fertilizer has increased from about 32 Tg N in 1970 to 80 Tg N in 1990. N fertilizer use is expected to increase to about 140 Tg N y^{-1} by 2050, with two-thirds of this being applied in developing countries (Galloway et al. 1995). Although these increases in N fertilizer use have been critical for increasing food production, they also have resulted in increased leaching losses, eutrophication, and trace-gas emissions (Vitousek et al. 1997). Most of the understanding of the consequences of fertilizer use for N trace-gas emissions stems from work in temperate zone, developed world agricultural systems. However, the shift in fertilizer use toward developing countries, where soils, climate, and management practices may be very different, suggests that greater focus on gas emissions and their controls is needed in these regions.

In this paper we focus on one impact of the large increase in global nitrogen (N) fertilizer use: the production of nitrous oxide (N_2O) during soil microbial denitrification. More than 70% of the anthropogenic N_2O source results form fertilized agriculture (IPCC 1995; Mosier et al. 1998). The microbial process of denitrification, which occurs in anaerobic soils, is a significant component of this source. Microbial nitrification, which occurs under aerobic conditions, also contributes to the agricultural N_2O source.

[1]Dept. of Civil and Environmental Engineering, 631 Davis Hall, University of California, Berkeley, CA 94720. Dr. Riley is corresponding author. E-mail: riley@nature.berkeley.edu

[2]Dept. of Geological and Environmental Sciences, Stanford University, Stanford, CA 94305.

Received April 15, 1999; accepted Oct. 13, 1999.

N_2O is an accumulating greenhouse gas and currently accounts for about 8% of the estimated anthropogenic contribution to global radiative forcing (IPCC 1995). Additionally, N_2O is stable in the troposphere, but upon reaching the stratosphere is responsible, in part, for the destruction of ozone. The dominant mechanism of N_2O destruction is photolysis in the stratosphere, resulting in a relatively long atmospheric life of about 120 years.

Several models exist that can predict N trace-gas emissions from agricultural soils, ranging from simple empirical representations to mechanistic treatments of processes responsible for N trace-gas emissions. Li et al. (1992) developed a multilayered model (DNDC) that predicts soil N cycling and trace-gas effluxes; they also presented a review of related models published through 1991. Grant et al. (1993a and b) described and tested a mechanistic model of N_2O effluxes from saturated, anaerobic soils. Parton et al. (1996) have developed a largely empirical model (NGAS) that correlates soil NO_3^- levels, respiration rates, moisture content, pH, temperature, and texture with N_2O and N_2 efflux estimates. Muller et al. (1997) also described an empirically based model of N_2O production via denitrification and nitrification based on soil NO_3^- and NH_4^+ levels, soil temperature, and soil moisture.

Our goal in developing the denitrification submodel described here was to improve on previous process models by including: (i) mechanistic treatments of the soil anaerobic fraction, denitrifier biomass dynamics, rates of soluble N transformations, and N_2O and N_2 fluxes within the soil profile; (ii) estimating gas effluxes to the atmosphere based on the surface concentration gradient; and (iii) estimating the model's predictive uncertainty based on input parameter and initial condition uncertainty. In addition to describing NLOSS's structure and its denitrification submodel, we present a preliminary investigation applying NLOSS to develop simplified predictors of N trace-gas speciation driven by readily available meteorological, edaphic, and management information. We intend to use NLOSS in future work to develop alternative management strategies that reduce the environmental consequences of intensive agriculture while maintaining the farmer's economic return.

METHODS

Microbial denitrification occurs under anaerobic conditions when denitrifying bacteria switch from using O_2 as an electrode acceptor to either NO_3^-, NO_2^-, or N_2O (Firestone and Davidson 1989). Soluble carbon provides the dominant source of electron donors during this process. The N_2O and N_2 molecules produced during denitrification can migrate between the aqueous and gaseous phases in the soil, diffuse through the soil as gases, and be emitted to the atmosphere. In this section we describe the NLOSS submodels designed to predict soil N_2O and N_2 production and efflux during denitrification, and the ^{15}N tracer experiment used to test the model.

Soil Moisture and Heat Transport

NLOSS simulates the transport of liquid water, vapor, and heat with a finite-difference discretization of a one-dimensional soil column. Riley et al. (2000) describe in detail the methods used in NLOSS to compute the transient soil water flux. Briefly, we apply a Richard's equation solution for transport of liquid water in the unsaturated soil. The bypass model of Eckersten and Jansson (1991) is included to account for water flow through macropores. Liquid and gaseous components of the water flux are coupled either by (i) calculation of a latent energy loss using the FAO Penman-Monteith technique (Allen et al. 1994), or (ii) modeling vaporization within the soil column and subsequent vapor transport (following Kondo and Saiguso (1994)). In this study, we apply both methods of computing the soil-surface vapor flux to determine the sensitivity of our results to the prediction of soil evaporation.

Riley et al. (2000) also describe our implementation of the FAO Penman-Monteith method of estimating evapotranspiration. In this submodel, NLOSS uses hourly measurements of net radiation, ground heat flux, air temperature, wind speed, and humidity to estimate the evapotranspirative flux. We apply the method of Rosenberg (1974) to reduce the evapotranspiration rate for very dry soils. The resulting "actual" evapotranspiration is partitioned into soil evaporation and transpiration by the methods described in Ritchie and Burnett (1971) and Hanks and Ritchie (1991). As described below, the data used in this paper to test the denitrification submodel were gathered during a pre-planting experiment (when fertilizers are typically applied in our Yaqui Valley test site). Under these conditions, the water vapor efflux consists solely of soil evaporation.

We base our second method of estimating the soil evaporative flux on the model of Kondo and Saiguso (1994). With this technique, the vapor content in the soil, q (kg kg^{-1}), is computed as

$$\frac{\partial((\theta_s - \theta)\rho_a q)}{\partial t} = \frac{\partial F_v}{\partial z} + E_v \qquad (1)$$

where θ is the soil water content (−), θ_s is the structural pore space (−), t is time(s), z is the depth

into the ground (m), E_v is the evaporation rate into the pore air (kg m^{-3} s^{-1}), ρ_a is air density (kg m^{-3}), and F_v is the vapor flux (kg m^{-2} s^{-1}), defined as:

$$F_v = D_a f \frac{\partial q}{\partial z} \quad (2)$$

Here D_a is the molecular diffusivity of vapor in air (m^2 s^{-1}), and f is a factor that accounts for the reduction in diffusive transport caused by soil grains and water (Millington 1959):

$$f = \epsilon^{4/3} \quad (3)$$

where ϵ is the air-filled porosity. The surface evaporative efflux Q_v (kg m^{-2} s^{-1}), is computed as a gradient-driven flux between the top soil layer and the atmosphere using a bulk transfer formula (Kondo and Saiguso, 1994):

$$Q_v = \rho_a C_E u\,(q(1) - q_a) \quad (4)$$

Here, C_E is the bulk transfer coefficient for vapor (−), u (m s^{-1}) is the wind speed, and $q(1)$ and q_a (kg kg^{-1}) are the vapor contents in the top soil layer and atmosphere, respectively.

In NLOSS the water transport equations are solved iteratively with a fully implicit temporal discretization. The solution procedure terminates when the computed values of θ at each point in the soil change fractionally by less than 10^{-4} over successive iterations. For the simulations presented here, we used the following measured hydrologic parameters from the Yaqui Valley site: saturated hydraulic conductivity = 2.5×10^{-6} m s^{-1}, saturated matric potential = −0.0616 m, and slope of the water retention curve = 9.5.

We compute the soil heat flux, F_H (J m^{-2} s^{-1}), assuming Fourier conduction:

$$F_H = -\lambda \frac{dT}{dz} \quad (5)$$

where λ (W m^{-1} K^{-1}) is the bulk thermal conductivity and T is the soil temperature (K). The DeVries model (1975) is used to approximate the bulk thermal conductivity:

$$\lambda = \frac{\theta\lambda_w + k_s(1-\theta)\lambda_s + k_a(\theta_s - \theta)\lambda_a}{\theta + k_s(1-\theta) + k_a(\theta_s - \theta)} \quad (6)$$

where λ_w, λ_s, and λ_a are the thermal conductivities of water, soil, and air, respectively (0.57, 0.3, and 0.025 W m^{-1} K^{-1}); and k_s and k_a are shape factors for soil and air, respectively (0.21 and 1.4). Equation (5) is discretized on the same vertical grid as the Richard's equation for water flux and solved with an analogous approach.

Anaerobic Fraction

Because microbial denitrification occurs under anaerobic conditions, a mechanistic treatment of denitrification should include an estimate of soil anaerobicity. We have included in NLOSS two models, based on two different idealizations of soil structure, to estimate the fraction of soil sufficiently anoxic for denitrification to occur. By coupling a soil anaerobicity submodel to NLOSS's representation of water, O_2, and C dynamics, we can predict the transient, vertically resolved anaerobic soil fraction.

The first anaerobicity model, based on Arah and Smith (1989), assumed that soil is comprised of spherical aggregates whose size and biological activity follow lognormal probability distributions. Within an aggregate, the biological consumption of oxygen follows Michaelis-Menten kinetics. The second model is based on the representation of Rijtema and Kroes (1991), which considers the soil to be randomly distributed cylindrical pores with uniform metabolic activity and zero-order reaction kinetics. Both of these models consider lognormal distributions for either pore or aggregate sizes and, therefore, implicitly allow for the development of microsite anaerobicity. Arah and Vinten (1995) provide functional relationships, based on statistical regressions of model results, to simplify inclusion of these two relatively complex techniques in ecosystem models. The regression exercises generated very good fits ($r^2 = 0.998$) for the simulated anaerobic fraction. When included in NLOSS, both simplified models produced comparable estimates of transient soil anaerobicity following a wetting event (rain or irrigation).

The results presented in this paper were produced using the Rijtema and Kroes soil model. For this case, the soil anaerobic fraction, ϕ (−), is estimated as

$$\phi = \exp\left(-a r_\psi^{-\alpha} V^{-\beta} O_2^{\gamma} [\theta + \chi\epsilon]^{\delta}\right) \quad (7)$$

where r_ψ is the radius (m) of a typical air-filled pore at moisture tension ψ (m), V is the O_2 reaction rate (mol m^{-3} s^{-1}), O_2 is the O_2 concentration in the pore air (mol m^{-3}), χ is the ratio between the molecular diffusivity of O_2 in air and water (−), and a, α, β, γ, and δ are constants determined by regressions to model output. V is estimated from the reaction potential, V_p (mol m^{-3} s^{-1}), and the amount of labile carbon at a particular soil depth (see Table 1 for values used in the simulation). Since it is a regression model, there is no physical significance to the structure of Eq. (7).

TABLE 1

Parameters used in the anaerobic fraction model using the soil conceptualization of Rijtema and Kroes (1991)

Parameter	Description	Units	Value
V_p	O_2 reaction potential	mol m^{-3} s^{-1}	20×10^{-6}
χ	Ration between the molecular diffusivity of O_2 in air and water		
$a, \alpha, \beta, \gamma, \delta$	Regression constants		1.5×10^{-6}, 1.26, 0.6, 0.6, 0.85

O_2 Transport and Consumption

We compute the O_2 flux, F_{O_2} (mol m^{-2} s^{-1}), within the soil profile assuming Fickian dynamics (notice the similarity to Eq. (2)):

$$F_{O_2} = D_{O_2} f \frac{\partial O_2}{\partial z} \tag{8}$$

where D_{O_2} is the temperature-dependent molecular diffusivity of O_2 in air (m^2 s^{-1}) (Camillo et al. 1983). The surface flux of O_2 into the soil is driven by the concentration gradient between the top soil layer and the atmosphere. In addition to soil transport, O_2 is consumed by microbes in the aerobic soil. This consumption, which establishes the soil O_2 deficit driving the surface flux, occurs at the rate V (defined above). Thus, following a wetting event, microbes consume O_2 in the aerobic fraction of soil, turning the soil anaerobic. The subsequent restoration of soil aerobicity occurs as a competition between microbial consumption of O_2 and the supply of atmospheric O_2 via diffusion from the soil surface.

Denitrification

Within the soil anaerobic fraction, microbial denitrification follows the reductive sequence: $NO_3^- \rightarrow NO_2^- \rightarrow N_2O \rightarrow N_2$. We base our microbial denitrification simulation on the model of Leffelaar and Wessel (1988); Li et al. (1992) have applied the same denitrifier kinetics in their DNDC model. NLOSS's denitrification submodel is summarized briefly in this section.

The denitrifier growth rates follow double-Monod kinetics, with the relative growth rate, μ_i (s^{-1}), for each step in the reductive sequence computed as:

$$\mu_i = \mu_i^m \frac{[C]}{K_c + [C]} \frac{[E_i]}{K_i + [E_i]} \tag{9}$$

Here, μ_i^m is the maximum relative growth rate (s^{-1}) on electron acceptor i (i = 1, 2, and 3 for NO_3^-, NO_2^-, and N_2O, respectively), C is the labile carbon concentration (kg C kg^{-1}), E_i is the concentration of electron acceptor i (kg N m^{-3}), and K_c and K_i are half-saturation constants for carbon and electron acceptor i, respectively (kg m^{-3}). The microbial consumption of soluble carbon is modeled with the Pirt (1965) equation:

$$\frac{dC}{dt} = \left(\frac{\mu}{Y_c} + m_c\right) B \tag{10}$$

where $\mu = \mu_1 + \mu_2 + \mu_3$. Consumption of electron acceptors is computed as:

$$\frac{dE_i}{dt} = \left(\frac{\mu_i}{Y_i} + m_i \frac{E_i}{E}\right) B \tag{11}$$

In Eqs. (10) and (11), Y_c and Y_i are maximum growth yields (kg C kg^{-1}) on soluble carbon and electron acceptor i, respectively; m_c and m_i are maintenance coefficients (kg kg^{-1} s^{-1}); E is the total mass of electron acceptors (kg N m^{-3}); and B is the mass of bacterial carbon (kg C). Thus, aqueous N_2O and N_2 concentrations are functions of the relative consumption rates as described by Eq. (11). For example, the contribution from denitrification to the aqueous N_2O concentration is computed as the difference between the production $\left(\frac{dE_2}{dt}\right)$ and consumption $\left(\frac{dE_3}{dt}\right)$ of N_2O. Denitrification produces aqueous N_2 at the rate $\left(\frac{dE_3}{dt}\right)$. Therefore, with this technique there is no need to estimate the ratio of N_2 to N_2O production.

The net rate of change of denitrifier biomass is computed as the difference between first order growth and death rates. The bacterial growth rate constant is based on the double Monod kinetics described by Eq. (9), whereas the death rate constant is based on carbon maintenance and growth yield coefficients. Following Leffelaar and Wessel (1988), we assumed that the initial biomass concentration of heterotrophic bacteria was 1×10^{-4} kg C kg

soil^{-1}; of this, the initial fraction of denitrifying bacteria was 2%. Soil N levels were initialized based on measurements made at the site. The initial labile carbon concentration in the near-surface soil was taken to be 25×10^{-6} kg C kg^{-1}, consistent with the low organic carbon content in the Yaqui Valley site and estimates presented in Li et al. (1992).

Estimates of nitrate assimilation, carbon and nitrogen mineralization, and immobilization of carbon and nitrogen are scaled to the growth and death rates of denitrifiers. NLOSS computes the time rate of change of each electron acceptor, for biological effects, as the sum of changes associated with microbial denitrification and microbial mineralization, assimilation, and immobilization. In the denitrification submodel of NLOSS, we use the constants derived directly from the literature as presented by Leffelaar and Wessel (1988); Table 2 presents these values. Comparisons between NLOSS's predictions under imposed conditions of 100% anaerobicity to results presented in Leffelaar and Wessel (1988) were excellent. The predicted development of denitrification products, under these conditions, were also consistent with the results of Cho (1982) and Cooper and Smith (1963).

Decomposition

NLOSS's prediction of soil carbon cycling is based on the decomposition model developed for DNDC (Li et al. 1992), which is derived from the model of Molina et al. (1983). These models are qualitatively similar to the CENTURY model of Parton et al. (1987). Because, as we show later, the time during which the soil is sufficiently anaerobic to support denitrification is short (~o(1 d)), decomposition during this period plays an insignificant role in affecting the N trace-gas effluxes. Therefore, we present only a short description of NLOSS's decomposition submodel.

Briefly, NLOSS models decomposition by dividing the soil carbon into three organic matter pools: residues, microbial biomass, and humus. These pools are further divided into labile and resistant fractions. Decomposition is treated as a pseudo-first order decay from each of these pools, where the rate constant is a function of the pool's potential decomposition rate, soil temperature, and soil moisture. Soil N cycling is tied to carbon transformations because each transfer of C requires a concurrent transfer of N. The varying C:N ratios of the soil pools cause C flow limitations to occur when there is insufficient N to complete the transfer. Conversely, surplus N from a C flow is returned to the soil mineral N pool. We estimate additions to the soluble C pool from fluxes out of the microbial and humads pools.

TABLE 2

Parameters used in the denitrification submodel of NLOSS (values are from Table 3, column 4 of Leffelaar and Wessel (1988)). Parameter definitions are given in the text and in the Nomenclature section.

Symbol	Substrate	Units	Parameter Value
$\mu_i \times 10^6$	NO_3^-	s^{-1}	4.8
	NO_2^-	s^{-1}	4.8
	N_2O	s^{-1}	2.4
$K_i \times 10$	C	kg C m^{-3} water	0.17
	NO_3^-	kg N m^{-3} water	0.83
	NO_2^-	kg N m^{-3} water	0.83
	N_2O	kg N m^{-3} water	0.83
$Y_i \times 10^2$	C	kg kg^{-1} C	50.3
	NO_3^-	kg kg^{-1} N	40.1
	NO_2^-	kg kg^{-1} N	42.8
	N_2O	kg kg^{-1} N	15.1
$m_i \times 10^5$	C	kg C kg^{-1} s^{-1}	0.21
	NO_3^-	kg N kg^{-1} s^{-1}	2.5
	NO_2^-	kg N kg^{-1} s^{-1}	0.97
	N_2O	kg N kg^{-1} s^{-1}	2.2

Aqueous and Gaseous Transport

Prediction of soluble compound and trace-gas transport is an important component of NLOSS. Soluble compound transport via advection is included in the mass balance of electron acceptors and carbon at each soil control volume. In NLOSS, the advective flux of soluble compound i, F_i (kg m^{-2} s^{-1}), is computed as

$$F_i = C_{w,i}Q \tag{12}$$

where $C_{w,i}$ is the aqueous concentration of compound i (kg m^{-3}) and Q is the bulk water flow (m^3 s^{-1}). For the simulations presented here, we ignore dispersion of soluble compounds.

N_2O and N_2 molecules produced in the soil water can diffuse to the open pore air. Currently, we assume instantaneous equilibrium between N gases in the soil water and air. NLOSS estimates the interfacial trace-gas flux by computing the impact of net microbial N_2O and N_2 production on the equilibrium gas concentrations. We apply equilibrium ratios for N_2 and N_2O of 0.01686 and 0.6788 m^3 gas m^{-3} water, respectively. The smaller equilibrium ratio for N_2, compared with N_2O, results in a substantially larger flux from the liquid to the gas phase. This effect contributes to a more rapid depletion of N_2 from the pore water and, thus, from the soil column.

Once present in the soil air, the gases diffuse vertically through the column to the atmosphere. We compute the gas diffusive flux analogously to

Eq. (8), using temperature-dependent diffusion coefficients. The efflux to the atmosphere is computed by evaluating Eq. (8) at the soil-atmosphere interface.

Monte Carlo Simulations

Each parameter and initial condition utilized in NLOSS is uncertain to some extent. We apply a Monte Carlo technique to estimate the impact of parameter and initial condition uncertainty on the model's predictions of N trace-gas fluxes. For this analysis, we assume lognormal distributions for the initial conditions and soil hydrologic and denitrification parameters. These distributions are derived from estimates of the geometric mean and standard deviation (GSD) of each parameter. We have not yet included the effect of parameter covariation (e.g., a relationship between the saturated matric potential and hydraulic conductivity) in this analysis. The Monte Carlo technique involves performing many simulations, each with a different set of parameters and initial conditions chosen based on the assumed probability distributions. A mean and uncertainty range for the parameter of interest (e.g., the N_2O efflux) are then computed from the ensemble simulation results.

A GSD of 1.2 was used for the probability distributions of the saturated hydraulic conductivity, saturated matric potential, slope of the water retention curve, initial conditions for soluble carbon and nitrate, and denitrifier kinetics parameters. The Monte Carlo results were computed from an ensemble of 200 model simulations. We report predictions of water-filled pore space (hereafter WFPS, calculated as the percent of pore volume occupied by water) and N trace-gas effluxes as the mean and standard deviation of these simulation results.

Field Experiment

Model testing takes advantage of an on-going field study in irrigated wheat fields in Sonora, Mexico, where farmers typically apply about 250 kg N ha^{-1} as urea or anhydrous ammonia, mostly prior to planting (Matson et al. 1998). We apply data collected during a pre-planting ^{15}N tracer study to test the model's prediction of denitrified N_2O and N_2 effluxes following an irrigation event; Panek et al. (1999) describe the experiment in detail. Soils in this area are coarse sandy clay mixed with montmorillonitic clay (classified typic clacicorthid), and have an average pH of 7.7 and 0.8% percent organic matter (Meisner et al. 1992). Briefly, replicated, paired soil plots were labeled with 25% a.e. $K^{15}NO_3$ or $(^{15}NH_4)_2SO_4$ at a rate of 7% of the existing pool of NO_3^- or NH_4^+, respectively. During the 12-day experiment, soil samples were taken to 15 cm depth, and gas effluxes were measured at mid-day using 25-cm enclosed chambers. Gas samples were removed from the headspace at 0, 10, 20, and 30 min with nylon syringes. N_2O gas samples were analyzed on a gas chromatograph with ECD. $^{15}N_2O$ and $^{15}N_2$ were analyzed on a continuous flow GC mass spectrometer. By comparing fluxes and isotopic signatures from the NO_3^- and NH_4^+ seeded plots, the N_2O efflux was partitioned into microbially denitrified and nitrified sources. Note that in this paper, these experimental results are used solely for model testing and not for model calibration.

RESULTS AND DISCUSSION

Hydrologic Model

Figure 1 compares NLOSS's WFPS predictions in the top 10 cm of soil to the experimentally measured values over the course of the ^{15}N tracer experiment. For these results, the Kondo technique of estimating the evaporative water flux was used. As is typical for a pre-plant irrigation in the Yaqui Valley, the soil was flooded by adding about 120 mm of water over a 6-h period. Similar excellent agreement with the WFPS data was found using the FAO Penman-Monteith technique to compute the evaporative water efflux.

Soil Anaerobic Fraction

Figure 2 shows NLOSS's estimates of the soil anaerobic fraction over the course of the experiment for 0–10, 10–20, 20–30, and 30–40-cm depth intervals. As the soil becomes saturated at the beginning of the experiment, microbes quickly consume the available O_2, turning the soil anaerobic. Development of anaerobicity begins in the top

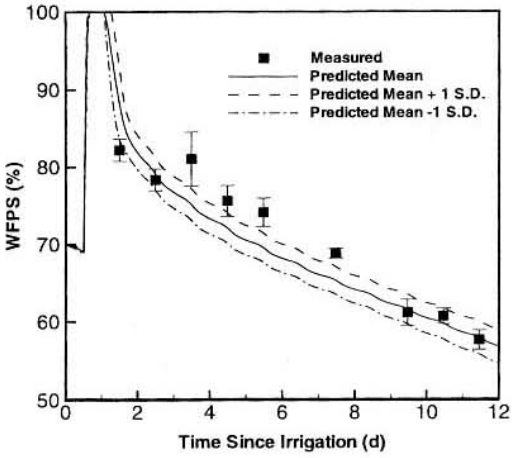

Fig. 1. WFPS predictions in the top 10 cm of soil over the course of the ^{15}N tracer experiment.

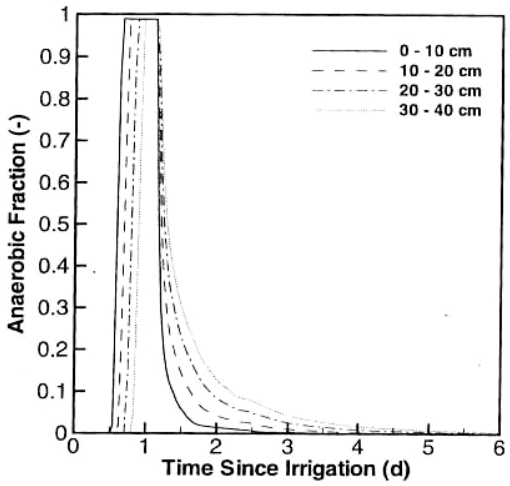

Fig. 2. Predictions of soil anaerobic fraction over the course of the ^{15}N tracer experiment for soil depths of 0–10, 10–20, 20–30, and 30–40 cm.

soil layer and then progresses downward, with about a 2-h delay to reach peak anaerobicity for every 10 cm of soil depth. This delay mirrors the time required for water to move through the column and saturate each successive layer. As the soil drains, O_2 diffuses into the profile from the surface, and the soil reoxygenates. As described by Eq. (7), the instantaneous values of oxygen concentration and soil water content control the predicted anaerobic fraction. Figure 2 indicates that the top 10 cm of soil returned to an aerobic state after 2 days. Thus, very little denitrification occurred in the top 10 cm of the soil after 2 days. Deeper in the profile, a portion of the soil remained anaerobic for up to 6 days. Unfortunately, because there is no effective technique to measure soil anaerobicity, we have no means to test this intermediate prediction.

Soil N Concentrations

In the anaerobic soil fraction, denitrifying microbes sequentially reduce aqueous NO_3^-, NO_2^-, and N_2O. Figures 3 (a), (b), and (c) show predicted concentrations of soil aqueous NO_3^-, N_2O, and N_2, respectively, over the 12-day field experiment. As soil anaerobicity develops, NO_3^- concentrations in the top soil layer decline rapidly. After about 1 day, the top soil layer NO_3^- pool has been depleted. The small peak in NO_3^-

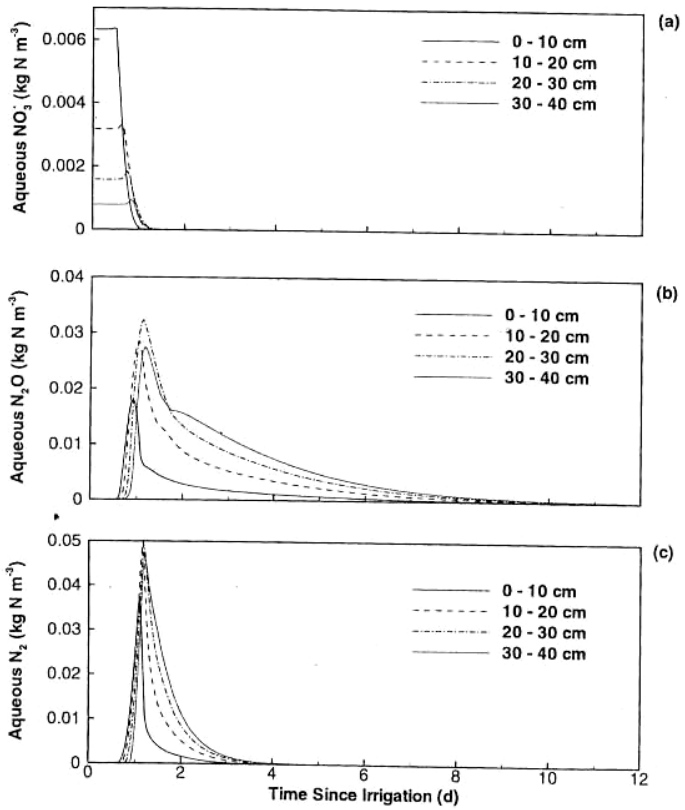

Fig. 3. Predicted concentrations of soil aqueous (a) NO_3^-, (b) N_2O, and (c) N_2 over the ^{15}N tracer experiment

concentrations during the first day in the lower soil layers results from NO_3^- leaching. Notice that this peak shifts about 2 h for every 10 cm of depth, corresponding to the time required for water to move through the column. Once the deeper layers turn anaerobic, the consumption of NO_3^- by denitrifiers reduces the soil NO_3^- concentrations substantially. Microbial consumption of NO_3^- halts when the soil returns to an aerobic state. As Fig. 2 indicates, soil aerobicity is restored between 2 and 6 days after irrigation, depending on the soil depth. Therefore, the impact of denitrifiers on the soil NO_3^- pool ceases after 2 to 6 days.

The rapid increase in aqueous N_2O (Fig. 3 (b)) at the beginning of the experiment results from the reduction of NO_3^- (Fig. 3 (a)) and NO_2^- (not shown). About 2 days following irrigation, very little N_2O is microbially produced or consumed in the denitrification process because the soil has returned to a mostly aerobic state. After this time, the decline in aqueous concentration is governed by transport between the aqueous and gaseous phases and subsequent diffusion through the soil column. Aqueous N_2 levels decline more rapidly than N_2O (Fig. 3 (c)), reflecting the large difference in equilibrium ratios.

The microbial production of aqueous N_2O and N_2 results in a gas flux into the open pore space; these gases then diffuse through the soil column and into the atmosphere. Figures 4 (a) and (b) show the predicted soil N_2O and N_2 gas concentrations, respectively, over the 12-day experiment. N_2O persists in the soil longer than N_2. N_2's smaller equilibrium ratio and larger gas diffusion coefficient result in more rapid movement between the aqueous and gaseous phases, through the soil and, therefore, to the atmosphere. Also, N_2O production continues longer than N_2 in the deeper soil layers, contributing to the more persistent N_2O soil-gas concentrations.

N Trace-Gas Fluxes

Figure 5 shows the measured and predicted N_2O fluxes from denitrification over the course

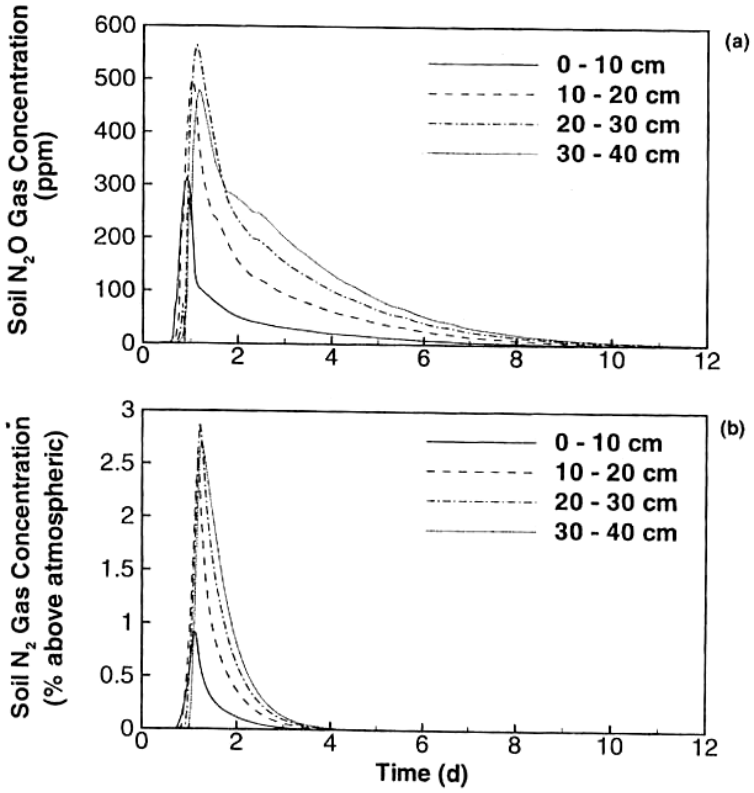

Fig. 4. Predicted soil (a) N_2O and (b) N_2 gas concentrations over the ^{15}N tracer experiment.

of the ^{15}N tracer experiment. The solid line is NLOSS's mean prediction for 200 Monte Carlo simulations; the individual symbols represent the measured fluxes. The two dashed lines bracketing the predicted mean represent 1 standard deviation of the Monte Carlo simulation results. Thus, parameter and initial condition uncertainty result in about a 30% uncertainty in the mean prediction for the peak denitrified N_2O flux (at about 2 days). Figure 5 demonstrates that NLOSS accurately predicted both the peak magnitude and temporal dynamics of the denitrified N_2O surface flux.

Measured and predicted N_2 effluxes are shown in Fig. 6; NLOSS also accurately simulated the magnitude and dynamics of the N_2 flux. Significantly, essentially identical N_2O and N_2 efflux predictions were obtained using the two methods of computing evapotranspirative flux, indicating that the gas efflux predictions are robust with respect to this calculation. The extent and dynamics of the trace-gas effluxes shown in Figs. 5 and 6 are consistent with experimental measurements made in irrigated corn and barley by Moiser et al. (1986). Finally, recall that the predicted N_2 flux results from production and transport within the soil column and is not computed as a fraction of the N_2O flux, as is common in many current trace-gas models.

The timing of the development of soil anaerobicity and N trace-gas effluxes implies that a substantial portion of the gas emitted to the atmosphere occurred well after microbial production of these gases had ceased. Model results suggest that the top 10 cm of soil had returned to an aerobic state about 2 days after irrigation (Fig. 2). Thus, production of denitrified N_2O and N_2 within the soil column early in the experiment led to effluxes up to 10 days later. The characteristic time, τ (s), for diffusive transport of N trace gases from depth to the soil surface is

$$\tau = \frac{L^2}{D} \tag{13}$$

where L is the depth into the soil (m) and D is the diffusion coefficient ($m^2\ s^{-1}$) corrected for porosity and soil moisture. The characteristic time for N_2O to diffuse to the surface from 30 cm depth (assuming a constant WFPS of 70%) is about 3 days. This time scale is consistent with the model's prediction that production of denitrified N trace gases ended between 2 and 6 days after irrigation, whereas diffusive soil effluxes persisted for up to 12 days.

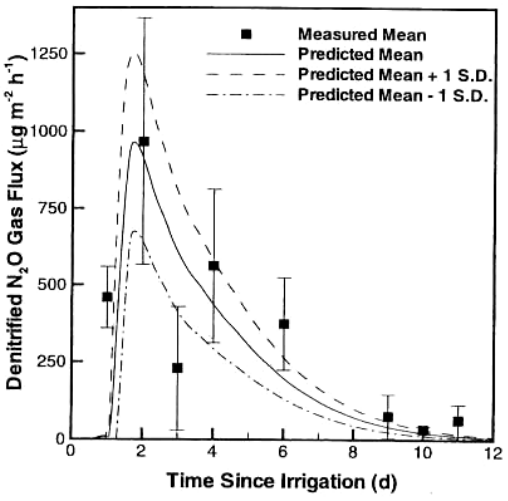

Fig. 5. Measured and predicted denitrified N_2O fluxes over the course of the ^{15}N tracer experiment.

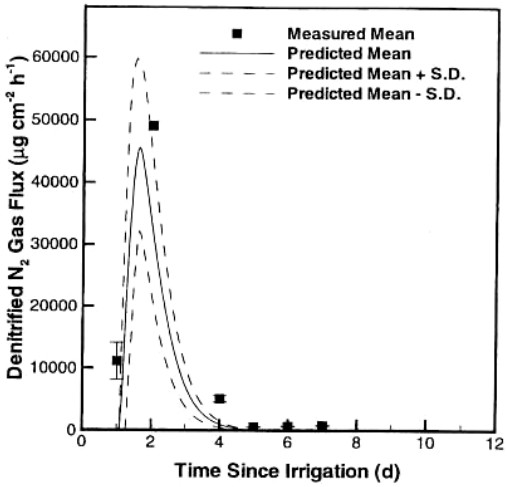

Fig. 6. Measured and predicted N_2 fluxes over the course of the ^{15}N tracer experiment. The peak measured N_2 flux was highly variable (see Panek et al. (1999)).

N Leaching

With the model we can examine the impact of leaching on soluble N concentrations and N trace-gas fluxes. For example, Fig. 7 shows the aqueous concentrations of soil NO_3^- for a simulation where advective aqueous transport has been suppressed. Notice that, in the top soil layer,

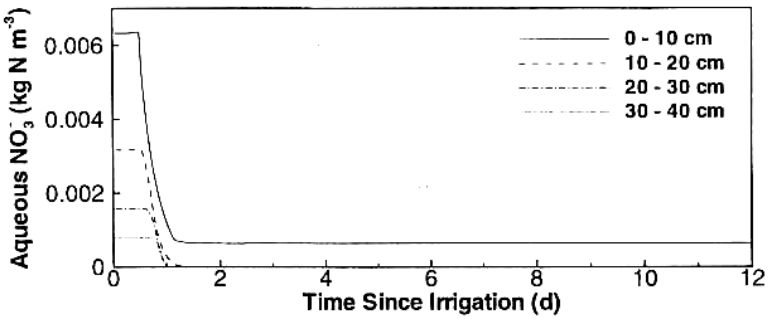

Fig. 7. Predicted aqueous concentrations of soil NO_3^- for an NLOSS simulation where advective aqueous transport has been suppressed.

the NO_3^- concentration does not become depleted. Thus, leaching is an important mechanism for transport of NO_3^- from the top soil layer, even over the short time during which the water flux exists in the experiment.

Soluble N leaching also affected the N_2O and N_2 gas effluxes. Comparing Figs. 3 (a) and 7 shows that the impact of leaching is to reduce top soil layer NO_3^- levels while slightly increasing NO_3^- concentrations at depth. N_2O production in the deeper soil layers is increased by these higher NO_3^- levels. Additionally, the impact of advective transport on N gas production is enhanced because the lower soil levels remain anaerobic substantially longer than the near surface soil. The net effect of NO_3^- leaching was to increase the integrated N_2O flux from denitrification over the 12 days by about 10%.

N Trace-Gas Speciation

Figure 8 presents NLOSS's predictions of the fraction of total N trace-gas emitted as either N_2O or N_2 during denitrification. The curves shown correspond to two soils: a sandy clay (typical of the Yaqui Valley) and a clay loam. Qualitatively, these curves follow the conceptualization used in the ecosystem model CASA (Potter et al. 1993) for computation of N trace-gas fluxes at high WFPS. When using that approach, the total N trace-gas efflux is assumed to be 2% of the estimated gross N mineralization rate. This rate is then partitioned into NO, N_2O, and N_2 gas fluxes based on WFPS. In CASA, with all else being equal, the same WFPS in different soils will result in the same speciation of N trace gases.

In contrast, Fig. 8 demonstrates that denitrified N trace-gas speciation depends on both WFPS and soil hydrologic parameters. This result occurs because the effluxes of N_2O and N_2 depend on the development of anaerobicity and substrate concentrations in addition to the soil water content. Soil-water anaerobicity depends on soil structure, soil-gas O_2 content, and WFPS, all of which are related non-linearly to soil hydrologic parameters. Therefore, development of anaerobicity following a wetting event will be a function of soil hydrologic properties. Also, substrate concentrations at any level in the soil column depend on water fluxes, which advect soluble compounds deeper into the profile. Since water fluxes depend on soil hydrologic properties, substrate concentrations will also be a function of these properties.

The advantages of the approach included in NLOSS and demonstrated here include the abil-

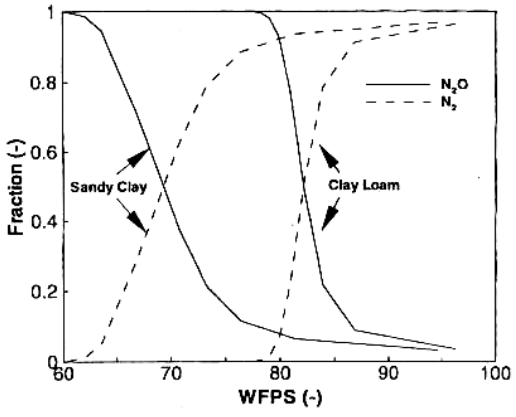

Fig. 8. Predicted fraction of the total N trace-gas emitted as either N_2O or N_2 during denitrification. The curves shown correspond to two soils: the sandy clays typical of the Yaqui Valley and a clay loam.

ity to mechanistically quantify the impacts of edaphic conditions, soil N levels, and fertilizer and irrigation management on denitrified N trace-gas speciation. In future work, we will apply these concepts to the development of field and regional scale models of N trace-gas emissions from soils.

CONCLUSIONS

NLOSS predicted the WFPS accurately over the course of the 12-day ^{15}N tracer experiment. Additionally, NLOSS predicted the soil moisture accurately at four soil depths over the course of a 6-month winter wheat season (data not shown). Accurate prediction of transient soil moisture content is critical for determining soil aerobicity, microbial transformation rates, and trace-gas transport and emission to the atmosphere.

In the simulated 12-day field experiment, soil anaerobicity developed shortly after irrigation, and the vertical development of anaerobicity followed the movement of water through the soil. In the top 10 cm, the soil returned to an aerobic state about 2 days after irrigation. Aerobicity was restored in the 30–40-cm layer after about 6 days. This result implies that in the top 10 cm of soil, denitrification ceases about 2 days after irrigation. Microbial denitrification and production of N_2O and N_2 continues for up to 6 days, however, in the deeper soil layers, and denitrified N_2O and N_2 emissions at the soil surface continue for up to 12 and 6 days, respectively, after irrigation. We demonstrated that these predicted results are consistent with the characteristic time required for a gas generated at depth to diffuse to the soil surface.

NLOSS predicted both the magnitude and temporal dynamics of the N_2O and N_2 gas effluxes accurately over the 12-day experiment. The Monte Carlo simulation results suggest that parameter and initial condition uncertainty resulted in about a 30% uncertainty in predicted N_2O and N_2 fluxes over the course of the experiment. About one half of the integrated N_2O and N_2 effluxes occurred after near-surface microbial denitrification had ceased. These fluxes result from gas production deeper in the soil column and subsequent diffusion to the surface. Although these conclusions are consistent with the experimental results described here, alternative hypotheses are possible. For example, if near-surface microsite anaerobicity were maintained substantially longer than NLOSS predicted, trace-gas fluxed comparable to those shown in Figs. 5 and 6 could occur from extended gas production in the near-surface soil.

The development of simplified models appropriate for regional and global simulations remains a goal of this research. Our preliminary investigations indicate that simplified models relying on daily WFPS, temperature, and inorganic N concentrations can be developed with NLOSS. In contrast to previous models, however, applying NLOSS to this problem allows us to account mechanistically for variations in edaphic conditions, land cover types, soil N levels, and fertilizer and water management strategies.

In addition, we have coupled NLOSS to CERES (a crop growth model, Hanks and Ritchie (1991)) to perform whole-season estimates of N trace-gas emissions from both nitrification and denitrification and leaching losses given specific management practices and environmental conditions. We intend to use this model to make recommendations to farmers that will allow them to reduce the environmental consequences of crop production while protecting their economic return on investment.

ACKNOWLEDGMENTS

The authors thank Ivan Ortiz-Monasterio, Jeanne Panek, and Tina Billow for their help throughout this project. This research was supported by grants from NASA's EOS Interdisciplinary Studies Program, the Kearney Foundation of Soil Science, and the University of California Campus-Laboratory Collaboration Program.

NOMENCLATURE

a	regression constant (−)
B	mass of bacterial carbon (kg C)
C	labile carbon concentration (kg C kg^{-1})
C_E	bulk transfer coefficient for vapor (−)
$C_{w,i}$	aqueous concentration of soluble compound i (kg m^{-3})
D	diffusion coefficient (m^2 s^{-1})
D_a	molecular diffusivity of vapor in air (m^2 s^{-1})
D_{O_2}	molecular diffusivity of O_2 in air (m^2 s^{-1})
E	total mass of electron acceptors (kg N m^{-3})
E_i	concentration of electron acceptor i (kg N m^{-3})
E_v	evaporation rate into the pore air (kg m^{-3} s^{-1})
f	reduction factor for diffusivity (−)

F_H soil heat flux (J m^{-2} s^{-1})
F_i advective flux of soluble compound i (kg m^{-2} s^{-1})
F_{O_2} O_2 flux (mol m^{-2} s^{-1})
F_v vapor flux (kg m^{-2} s^{-1})
k_a shape factor for air (−)
K_c half-saturation constant for carbon (kg m^{-3})
K_i half-saturation constant for electron acceptor i (kg m^{-3})
k_s shape factor for soil (−)
L depth into the soil (m)
m_c maintenance coefficient (kg kg^{-1} s^{-1})
m_i maintenance coefficient (kg kg^{-1} s^{-1})
O_2 O_2 concentration in the pore air (mol m^{-3})
q vapor content in the soil (kg kg^{-1})
Q bulk water flow (m^3 s^{-1})
q_a vapor content in the atmosphere (kg kg^{-1})
Q_v surface evaporative efflux (kg m^{-2} s^{-1})
r_ψ radius of a typical air-filled pore (m)
t time (s)
T soil temperature (K)
u wind speed (m s^{-1})
V O_2 reaction rate (mol m^{-3} s^{-1})
V_p O_2 reaction potential (mol m^{-3} s^{-1})
Y_c maximum growth yield on soluble carbon (kg C kg^{-1})
Y_i maximum growth yield on electron acceptor i (kg C kg^{-1})
z depth into the ground (m)

Greek letters
$\alpha, \beta, \gamma, \delta$ regression constants (−)
ϵ air-filled porosity (−)
ϕ soil anaerobic fraction (−)
$\lambda_w, \lambda_s, \lambda_a$ thermal conductivities of water, soil, and air, respectively (W m^{-1} K^{-1})
λ bulk thermal conductivity (W m^{-1} K^{-1})
μ growth rate (s^{-1})
μ_i relative growth rate on electron acceptor i (s^{-1})
μ_i^m maximum relative growth rate on electron acceptor i (s^{-1})
χ ratio between the molecular diffusivity of O_2 in air and water (−)
ρ_a air density (kg m^{-3})
θ soil water content (−)
θ_s structural pore space (−)
τ characteristic time (s)
ψ moisture tension (m)

Note: (−) denotes a dimensionless parameter

REFERENCES

Allen, R.G., M. Smith, A. Perrier and L.S. Pereira. 1994. An update for the definition of reference evapotranspiration. ICID Bull. 43:1–92.

Arah, J. R. M., and K. A. Smith. 1989. Steady-state denitrification in aggregated soils: A mathematical model. J. Soil Sci. 40:139–149.

Arah, J. R. M., and A. J. A. Vinten. 1995. Simplified models of anoxia and denitrification in aggregated and simple-structured soils. Eur. J. Soil Sci. 46:507–517.

Camillo, P. J., R. J. Gurney, and T.J. Schmugge. 1983. A soil and atmosphere boundary layer model for evapotranspiration and soil moisture studies. Water Resour. Res. 19:371–380.

Cho, C. M. 1982. Oxygen consumption and denitrification kinetics in soil. Soil Sci. Soc. Am. J. 46: 756–762.

Cooper, G.S., and R.L. Smith. 1963. Sequence of products formed during denitrification in some diverse western soils. Soil Sci. Soc. Am. Proc. 27:-659–662.

deVries, D. A., and N. H. Afgan. 1975. Heat and mass transfer in the biosphere. Scripta Book Co., New York.

Eckersten, H., and P. E. Jansson. 1991. Modeling water flow, nitrogen uptake and production for wheat. Fert. Res. 27:313–329.

Firestone, M. K., and E. A. Davidson. 1989. Microbiological basis of NO and N_2O production and consumption in soil. In: Exchange of Trace Gases between Terrestrial Ecosystems and the Atmosphere. M. O. Andreae and D. S. Schimel (eds.). John Wiley & Sons, London.

Galloway, J.N., W.H. Schlesinger, H. Levy, A. Michaels, and J.L. Schnoor. 1995. Nitrogen fixation-anthropogenic enhancement-environmental response. Global Biochem. Cycles 9:235–252.

Grant, R.F., M. Nyborg, and J.W. Laidlaw. 1993a. Evolution of nitrous oxide from soil: I. Model development. Soil Sci. 156:259–265.

Grant, R.F., M. Nyborg, and J.W. Laidlaw. 1993b. Evolution of nitrous oxide from soil: II. Experimental results and model testing. Soil Sci. 156: 266–277.

Hanks, J., and J. R. Ritchie. 1991. Modeling plant and soil systems. ASA, Madison, WI.

IPCC. 1995. Climate change 1995. The science of climate change. Press Syndicate of the University of Cambridge, New York.

Kondo, J., and N. Saiguso. 1994. Modeling the evaporation from bare soil with a formula for vaporization in the soil pores. J. Meteorol. Soc. JPN 72:413–420.

Leffelaar, P. A., and W. W. Wessel. 1988. Denitrification in a homogeneous, closed system: Experiment and simulation. Soil Sci. 146:335–349.

Li, C., S. Frolking, and T. Frolking. 1992. A model of nitrous oxide evolution from soil driven by rainfall events: 1. Model structure and sensitivity. J. Geophys. Res. 97:9759–9776.

Matson, P.A., R. Naylor, and I. Ortiz-Monasterio. 1998. Integration of environmental, agronomic, and economic aspects of fertilizer management. Science 280:112–115.

Meisner, C. A., E. Acevedo, D. Flores, K. Sayre, I. Ortiz-Monasterio, D. Byerlee, and A. Limon. 1992. Wheat production and grower practices in the Yaqui Valley, Sonora, Mexico. Wheat Special Report No. 6. CIMMYT (Centro Internacional de Mejoramiento de Maiz y Trigo).

Millington, R. J. 1959. Gas diffusion in porous media. Science 130:100–102.

Molina, J. A., C. E. Clapp, M. J. Shaffer, F. W. Chichester, and W. E. Larson. 1983. NCSOIL, a model of nitrogen and carbon transformation in soil: Description, calibration, and behavior. Soil Sci. Soc. Am. J. 47:85–91.

Mosier, A., C. Kroeze, C. Nevison, O. Oenema, and and others. 1998. Closing the global N_2O budget: Nitrous Oxide emissions through the agricultural nitrogen cycle—OECD/IPCC/IEA phase II development of IPCC guidelines for national greenhouse gas inventory methodology. Nutri. Cycl. Agroecosyst. 52:225–248.

Mosier, A. R., W. D. Guenzi, and E. E. Schweizer. 1986. Soil losses of dinitrogen and nitrous oxide from irrigated crops in northeastern Colorado. Soil Sci. Soc. Am. J. 50:344–348.

Muller, C., R. R. Sherlock, and P. H. Williams. 1997. Mechanistic model for nitrous oxide emission via nitrification and denitrification. Biol. Fertil. Soils 24:231–238.

Panek, J. A., P. A. Matson, I. Ortiz-Monasterio, and P. Brooks. 1999. Distinguishing nitrification and denitrification sources of N_2O in a Mexican wheat system using ^{15}N as a tracer. Ecol. Appl. (*in press*).

Parton, W. J., A. R. Mosier, D. S. Ojima, D. W. Valentine, D.S. Schimel, K. Weier, and A.E. Kulmala. 1996. Generalized model for N_2 and N_2O production from nitrification and denitrification. Glogal Biogeochem. Cycles 10:401–412.

Parton, W. J., D. S. Schimel, C. V. Cole, and D. S. Ojima. 1987. Analysis of factors controlling soil organic matter levels in Great Plains grasslands. Soil Sci. Soc. Am. J. 51:1173–1179.

Pirt, S. J. 1965. The maintenance energy of bacteria in growing cultures. Proc. R. Soc. London, Ser. B 163:224–231.

Potter, C. S., J. T. Randerson, C. B. Field, P. A. Matson, P. M. Vitousek, H. A. Mooney, and S. A. Klooster. 1993. Terrestrial ecosystem production: A process model based on global satellite and surface data. Global Biogeochem. Cycles 7:811–841.

Rijtema, P.E., and J.G. Kroes. 1991. Some results of nitrogen simulations with the model ANIMO. Fert. Res. 27:189–198.

Riley, W. J., I. Ortiz-Monasterio, and P. A. Matson. 2000. Nitrogen Leaching and Soil Nitrate, Nitrite, and Ammonium Levels Under Irrigated Wheat in Northern Mexico. (*in press*).

Ritchie, J. T., and E. Burnett. 1971. Dryland evaporation flux in a subhumid climate, 2, Plant influences. Agron. J. 63:56–62.

Rosenberg, N. J. 1974. Microclimate: The biological environment. John Wiley. New York.

Vitousek, P.M., J.D. Aber, R.W. Howarth, G.E. Likens, and others. 1997. Human alteration of the global nitrogen cycle: Sources and consequences. Ecol. Appl. 7:737–750.